NANO LETTERS
Cite This: Nano Lett. 2018, 18, 2343−2350
Letter
pubs.acs.org/NanoLett

Nanowires Bending over Backward from Strain Partitioning in Asymmetric Core−Shell Heterostructures

Ryan B. Lewis,* Pierre Corfdir,† Hanno Küpers, Timur Flissikowski, Oliver Brandt, and Lutz Geelhaar

Paul-Drude-Institut für Festkörperelektronik, Hausvogteiplatz 5−7, 10117 Berlin, Germany

Supporting Information

ABSTRACT: The flexibility and quasi-one-dimensional nature of nanowires offer wide-ranging possibilities for novel heterostructure design and strain engineering. In this work, we realize arrays of extremely and controllably bent nanowires comprising lattice-mismatched and highly asymmetric core−shell heterostructures. Strain sharing across the nanowire heterostructures is sufficient to bend vertical nanowires over backward to contact either neighboring nanowires or the substrate itself, presenting new possibilities for designing nanowire networks and interconnects. Photoluminescence spectroscopy on bent-nanowire heterostructures reveals that spatially varying strain fields induce charge carrier drift toward the tensile-strained outside of the nanowires, and that the polarization response of absorbed and emitted light is controlled by the bending direction. This unconventional strain field is employed for light emission by placing an active region of quantum dots at the outer side of a bent nanowire to exploit the carrier drift and tensile strain. These results demonstrate how bending in nanoheterostructures opens up new degrees of freedom for strain and device engineering.

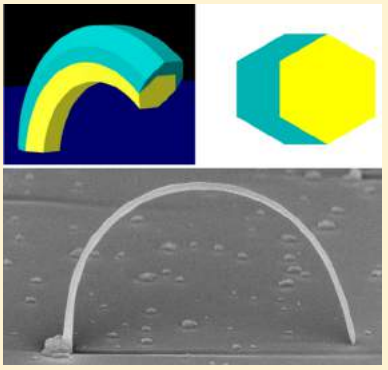

KEYWORDS: *Nanowires, semiconductors, strain engineering, heterostructures, optical characterization, bending*

Strain has always been a double-edged sword for heterostructure design, on the one hand constraining which materials can be combined to form coherent structures but on the other hand providing a means to modify materials properties by strain engineering. In conventional planar heterostructures, biaxial strain arising from lattice mismatch between the substrate and layers has been exploited to improve the performance of optoelectronic and electronic devices.[1,2] Apart from biaxial strain, realizing more complex spatially varying strain fields opens up new possibilities for strain engineering and provides a means to control the motion of charge carriers.[3−7] Along these lines, strain fields in microwires and nanowires which have been dispersed and subsequently mechanically bent have been shown to induce charge carrier drift toward the tensilely strained outside region of the wire.[7−10] Mechanical bending has also been used to fabricate nanowire field-effect transistor bioprobe arrays.[11] In addition to mechanical bending, spontaneous bending has been observed in lattice-mismatched core−shell nanowire heterostructures, and this has been attributed to asymmetric shell growth inducing asymmetric strain in the nanowire core.[12−17] However, the opportunities for strain and nanostructure engineering offered by bent-nanowire heterostructures have remained unexplored.

In this work, we investigate the controlled synthesis, optical properties, and device possibilities of bent-nanowire heterostructures. GaAs-based nanowires are bent in predetermined directions by strain sharing with asymmetric and lattice-mismatched $Al_{0.5}In_{0.5}As$ shells, which are deposited on a single side of the nanowires. This approach enables vertical nanowires to be bent over backward to contact either neighboring nanowires or the substrate, presenting a new way to form nanowire networks and nanowire electrical/optical interconnects. Photoluminescence (PL) spectroscopy reveals that spatially varying strain fields in the core of bent-nanowire heterostructures induce the drift of photoexcited charge carriers toward the tensilely strained outer part of the nanowire. Additionally, the bending direction determines the polarization response of absorbed and emitted light. We exploit the strain fields within bent nanowires to enhance the emission intensity of quantum dots (QDs) embedded within the nanowires by more than an order of magnitude. These findings open up a wide range of possibilities for designing new devices based on bent nanowires.

Nanowires have been explored as nanosubstrates in core−shell nanowire heterostructures,[18] which have been shown to elastically accommodate higher lattice mismatches than what is possible with conventional planar heterostructures.[19−23] For the synthesis of core−shell nanowires using directional deposition techniques such as molecular beam epitaxy (MBE), the substrate is typically rotated to facilitate uniform shell growth. The result is that strain induced in the core from lattice-mismatched shells is symmetric, and so the nanowires remain straight. In contrast to this common approach, we

Received: December 12, 2017
Revised: February 22, 2018
Published: March 23, 2018

DOI: 10.1021/acs.nanolett.7b05221
Nano Lett. 2018, 18, 2343−2350

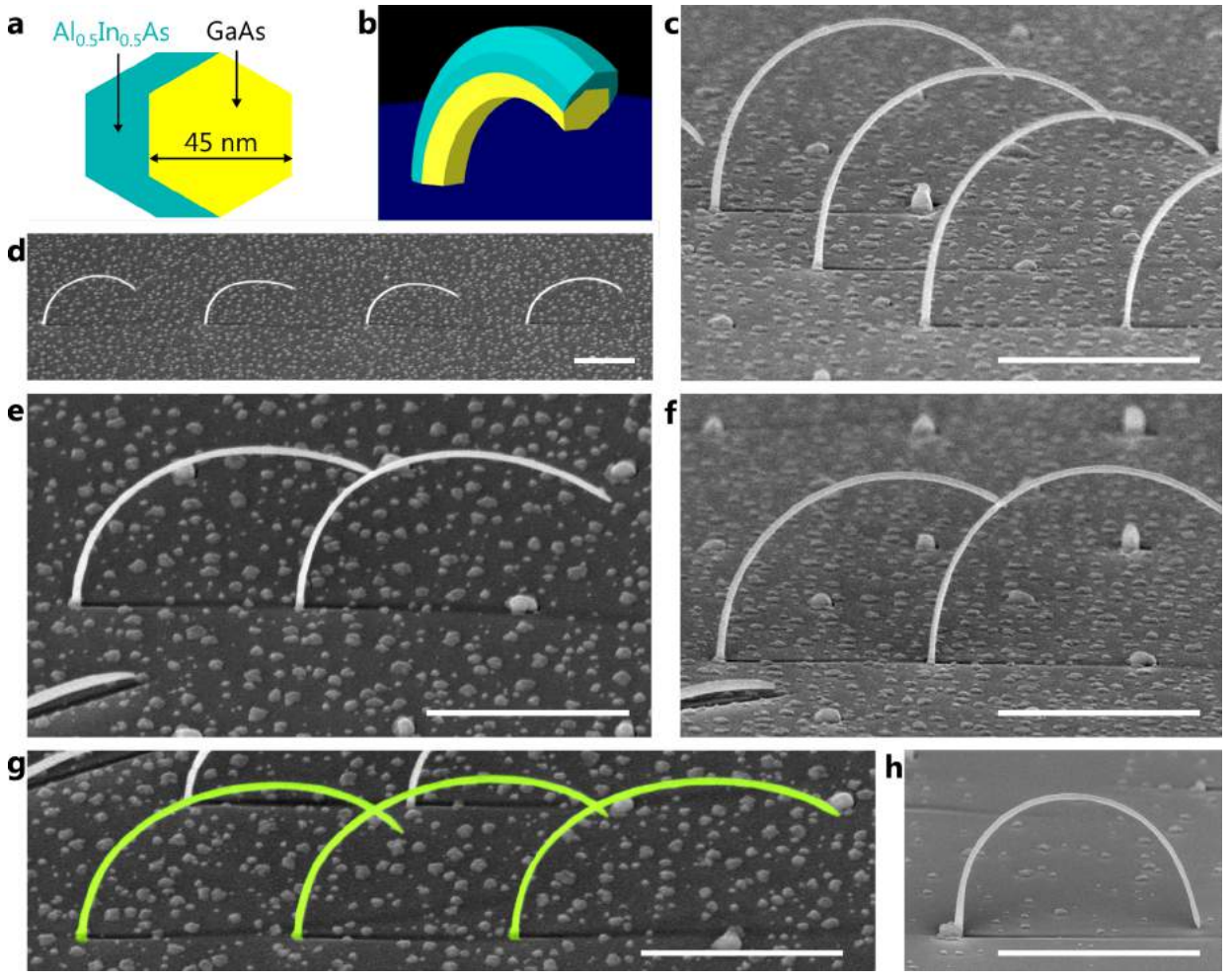

Figure 1. As-grown bent nanowires and nanowire chains. (a,b) Schematic representation of the nanowire structure, which consists of a 45 nm diameter GaAs core and a 20 nm $Al_{0.5}In_{0.5}As$ shell deposited on one side of the core. (c,d) SEM images of isolated bent nanowires taken at viewing angles of (c) 20° and (d) 45° from the substrate plane. (e,f) Images of the same two connected nanowires taken at viewing angles of (e) 45° and (f) 20° from the substrate plane. (g) A chain of three nanowires (45° viewing angle). (h) A nanowire with a thinner 30 nm core, bent completely over and contacting the substrate (20° viewing angle). In all SEM images, suppression of the parasitic growth by the nanowires is visible on the substrate due to the shadowing of the group III fluxes by the nanowire. The shadowing corresponds to the projection of the nanowire bending direction on the substrate plane, which is approximately the $[1\bar{1}0]$ direction. The scale bars corresponds to 2 μm in all panels and the viewing angle is from the $[2\bar{1}\ \bar{1}]$ direction.

synthesized GaAs/$Al_{0.5}In_{0.5}As$ core−shell nanowires at conditions chosen to maximize the asymmetry of the lattice-mismatched $Al_{0.5}In_{0.5}As$ shell, which has a larger bandgap than the GaAs core.[24] Namely, the $Al_{0.5}In_{0.5}As$ shells were grown as a "digital alloy" by MBE, whereby the substrate rotation and Al and In fluxes were sequenced in order to deposit both Al and In on the same side of the nanowires (see Methods). The GaAs-$Al_{0.5}In_{0.5}As$ lattice mismatch is expected to be at the upper limit of what can be accommodated coherently for these nanowire cores.[23]

Figure 1 presents scanning electron microscopy (SEM) images of GaAs/$Al_{0.5}In_{0.5}As$ core−shell nanowires with respective core diameter and shell thickness of 45 and 20 nm, selectively grown on prepatterned substrates. Schematic representations of the nanowire structure are shown in Figure 1a,b. The bent nanowires in Figure 1c,d, which were straight and standing vertically before $Al_{0.5}In_{0.5}As$ deposition (see Supporting Information (SI)), are bent by more than 90° away from the substrate normal. These nanowires have a bending radius of 1.68 ± 0.06 μm (10 wires measured) and are bent away from the direction from which the group-III fluxes impinged during shell deposition (see SI for top-view images). We note that GaAs nanowires bent in a predetermined direction by depositing MnAs shells by MBE have been previously reported although with a lower degree of bending.[12] The bending is a result of strain sharing between the GaAs core and the asymmetric $Al_{0.5}In_{0.5}As$ shell, which has a lattice mismatch of 3.6% from GaAs. Analytical strain calculations for the coherently strained structure shown in Figure 1a predict a similar bending radius of 1.3 μm (see SI), thus confirming that the actual core−shell structure is similar to the nominal one. The larger actual bending radius could be explained by the deviations from the nominal structure (e.g., core/shell thicknesses or shell composition) or the presence of plastic relaxation. For the strain calculations, the strain energy was minimized with respect to the bending radius and average strain state within the nanowire, considering only the strain component parallel to the nanowire axis $\varepsilon_{\parallel}$, which is the relevant component for bending. In general, our calculations show that for a nanowire with core diameter d_{core}, the minimum

DOI: 10.1021/acs.nanolett.7b05221
Nano Lett. 2018, 18, 2343−2350

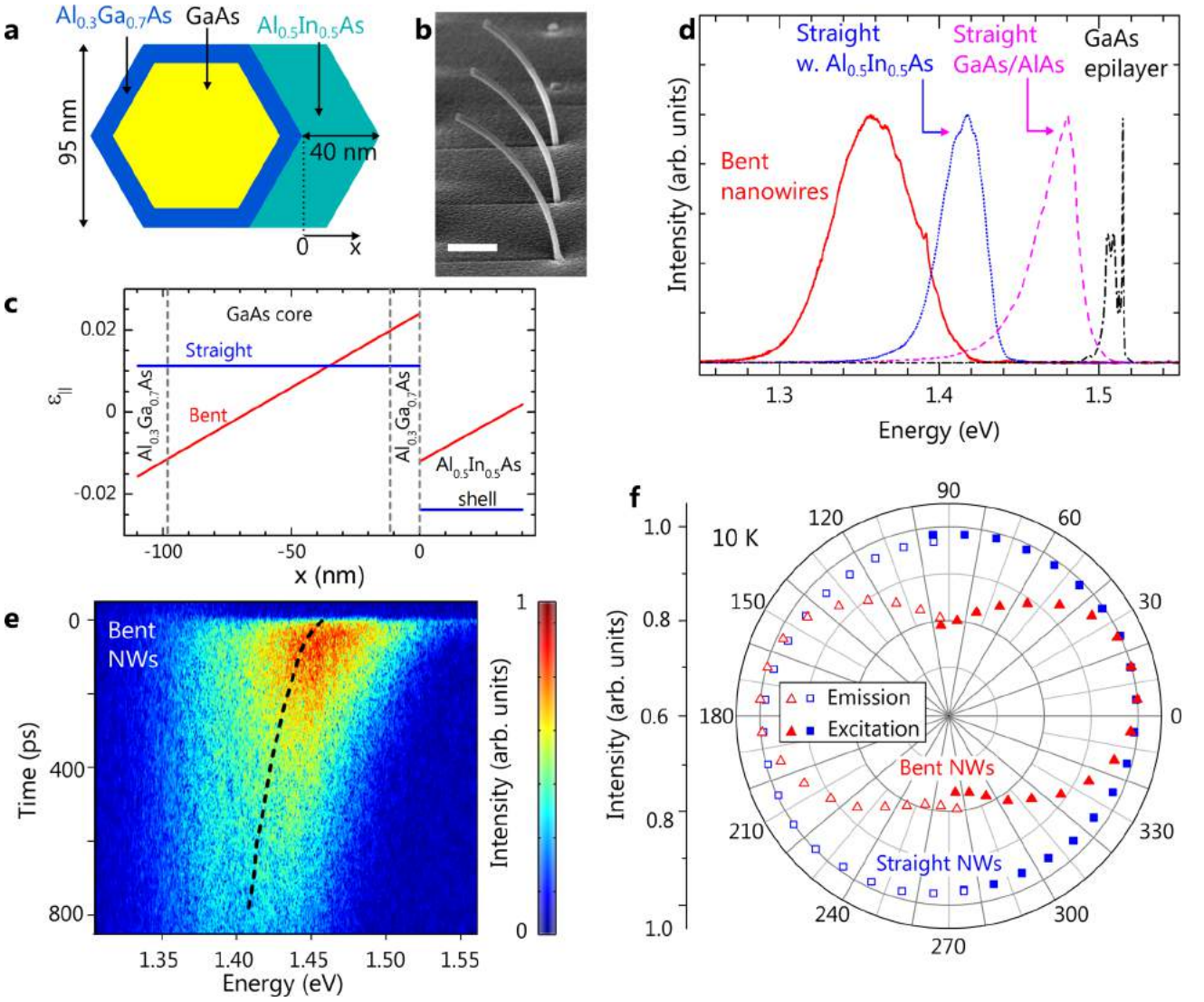

Figure 2. Charge carrier drift and optical polarization response of bent nanowires. (a) Schematic cross-section of the bent GaAs/$Al_{0.3}Ga_{0.7}As$/$Al_{0.5}In_{0.5}As$ core−multishell nanowires investigated in PL experiments. The $Al_{0.3}Ga_{0.7}As$ and $Al_{0.5}In_{0.5}As$ shells act as surface passivation and bending shells, respectively. (b) SEM image of bent selective area grown nanowires with the structure in (a) (viewing angle 20° from the substrate plane). The scale bar corresponds to 1 μm. (c) Axial strain variation along the x-axis in panel (a) for the straight and bent GaAs/$Al_{0.3}Ga_{0.7}As$/$Al_{0.5}In_{0.5}As$ core−multishell nanowires (blue and red lines, respectively) for a line crossing through the center of the core. (d) Normalized PL spectra at 10 K from a GaAs epilayer (black dashed-dotted line), an ensemble of GaAs/AlAs/GaAs nanowires (pink dashed line) and ensembles of straight and bent GaAs/$Al_{0.3}Ga_{0.7}As$/$Al_{0.5}In_{0.5}As$ nanowires (blue dotted line and red line, respectively). The excitation power was 1.4 μW. (e) Streak camera image taken on the bent nanowires at 10 K. The evolution of the PL peak energy extracted from Gaussian fits is shown as a dashed line. (f) Polar representation of the PL intensity from bent (red) and straight (blue) GaAs/$Al_{0.3}Ga_{0.7}As$/$Al_{0.5}In_{0.5}As$ core−multishell nanowires (NWs) at 10 K (hollow symbols). The filled symbols show the dependence of the PL intensity at 10 K on the polarization of the incident laser. For the bent nanowires, an angle of 0° corresponds to the bending direction of the nanowires.

bending radius r_{min} is achieved with a shell thickness of $0.45d_{core}$, and r_{min} increases linearly with increasing d_{core} ($r_{min} \approx 30d_{core}$ for the GaAs/$Al_{0.5}In_{0.5}As$ structure). Figure 1e,f illustrates a pair of connected nanowires from two viewing angles. Additionally, the three nanowires exhibited in Figure 1g show that multiple nanowires can also be connected in chains. These micrographs demonstrate that bending nanowires by more than 90° in controlled directions opens up new ways to engineer connected nanowire networks. This approach provides great design freedom, as the bending direction is simply determined by the side of the nanowires that the incident fluxes impinge on (see SI). Previous demonstrations of nanowire junctions have been based on tilted or branched straight nanowires, which are restricted to certain crystallographic directions.[25−30] Finally, Figure 1h shows a micrograph of a nanowire from a different sample with a thinner 30 nm diameter core, bent completely over to contact the substrate (bending radius about 1.1 μm). This striking effect could be exploited to fabricate electrical nanointerconnects (especially if metals are used) or possibly optical interconnects if thicker/longer nanowires (suitable for guiding light) are used. In the latter case, it could be possible to subsequently thicken the nanowires after interconnection. Additionally, the ability to form electrical/optical connections to the distal end of a nanowire could be exploited to contact nanowire devices (e.g., to form electrical contacts to nanowire light emitting diodes). The bending of nanowires by 90° and 180° requires nanowires

DOI: 10.1021/acs.nanolett.7b05221
Nano Lett. 2018, 18, 2343−2350

with lengths of at least $\frac{\pi}{2}r_{min}$ and πr_{min}, respectively. As r_{min} is limited by the nanowire core thickness, the aspect ratio of the core limits how much a nanowire can be bent. Specifically, a bending angle of 90° (the minimum for contacting nanowires) requires an aspect ratio greater than 45.

We now turn our attention to the spatially varying strain fields in nanowires bent by lattice-mismatched-asymmetric shells and how these fields affect the transport and radiative recombination of photogenerated carriers in the GaAs core. In order to minimize recombination at the surface and at the highly lattice-mismatched interface with the bending region, the surface of 75 nm diameter GaAs cores was passivated with a symmetric and nearly lattice-matched 10 nm thick $Al_{0.3}Ga_{0.7}As$ shell before being bent by a 40 nm thick $Al_{0.5}In_{0.5}As$ layer, as depicted schematically in Figure 2a. For this geometry, we calculate a radius of curvature of the bent nanowires of about 3 μm, similar to the experimental value of 3.4 ± 0.1 μm (see SI for additional images). SEM images reveal an average nanowire thickness of 128 ± 6 nm (Figure 2b), slightly less than the nominal 135 nm. The PL properties of these nanowires are compared with that of a straight $GaAs/Al_{0.3}Ga_{0.7}As/Al_{0.5}In_{0.5}As$ core−multishell nanowire sample with symmetric $Al_{0.5}In_{0.5}As$ shells with roughly the same volume as for the bent nanowires. Figure 2c shows the evolution of the tangential strain $\varepsilon_{\parallel}$ across the center of the nanowire section computed for the straight and the bent nanowires with the nominal structure. For both types of nanowires, the strain is shared by the core and the shells. However, while the GaAs core of straight nanowires exhibits a constant tensile strain parallel to the nanowire axis $\varepsilon_{\parallel}$ = 0.012,[19,22] $\varepsilon_{\parallel}$ varies linearly across the core of the bent nanowires from −0.011 to 0.020 between the inner and outer sides of the GaAs core, respectively (see SI for calculation).

The continuous-wave PL spectra of straight and bent $GaAs/Al_{0.3}Ga_{0.7}As/Al_{0.5}In_{0.5}As$ core−multishell nanowires at 10 K are displayed in Figure 2d. Spectra taken under the same conditions on a GaAs epilayer and GaAs/AlAs/GaAs core−multishell nanowires with symmetric shells are also shown. The spectrum for the epilayer is dominated by a donor-bound exciton transition at 1.515 eV, as expected for strain-free GaAs.[31] Although the GaAs/AlAs/GaAs core−multishell nanowires are also strain-free, the PL signal from the GaAs core is red-shifted,with a peak energy of 1.48 eV. Such a redshift arises from the presence of stacking defects that localize carriers along the nanowire axis at low temperatures.[32] The PL peak energies for the straight and bent $GaAs/Al_{0.3}Ga_{0.7}As/Al_{0.5}In_{0.5}As$ core−multishell nanowires are 1.417 and 1.357 eV, respectively, corresponding to a redshift compared to the GaAs/AlAs/GaAs core−multishell sample. This is consistent with the fact that the $Al_{0.5}In_{0.5}As$ shell induces tensile strain in the GaAs core. Note that the inhomogeneous strain across the bent GaAs cores (Figure 2c) leads to a distribution in PL energies (see SI for bandgap calculations). Accordingly, the PL band for the sample with bent nanowires exhibits a full width at half-maximum (fwhm) nearly twice that for the straight nanowire sample (59 and 31 meV, respectively, see Figure 2d).

The GaAs PL signal for the bent nanowires is clearly redshifted compared to that of the straight $GaAs/Al_{0.3}Ga_{0.7}As/Al_{0.5}In_{0.5}As$ core−multishell nanowires (Figure 2d), despite both samples containing similar amounts of $Al_{0.5}In_{0.5}As$. We note that the average core strain is actually lower in the bent nanowires, as can be seen in Figure 2c. One could expect to have detected light from carriers recombining at core regions under compression, that is, light at energies higher than those observed for the GaAs/AlAs/GaAs nanowires. The absence of such a signal suggests that in bent nanowires, photogenerated charge carriers drift from compressively to tensilely strained regions of the core. To evaluate the efficacy of this drift, we performed time-resolved photoluminescence experiments at 10 K. A streak camera image taken on the bent $GaAs/Al_{0.3}Ga_{0.7}As/Al_{0.5}In_{0.5}As$ core−multishell nanowires is shown in Figure 2e. Time-resolved spectra extracted from this image are provided in the SI, and the time evolution of the PL peak energy is shown as the dashed line in Figure 2e. For time delays below 50 ps, the PL spectrum exhibits a fwhm of 129 meV and covers energies below and above those observed for the straight strain-free GaAs/AlAs/GaAs nanowires (see Figure 2d). Carrier recombination thus occurs in both tensile- and compressively strained regions of the GaAs core. With increasing time delay, the PL signal redshifts and narrows, an observation consistent with the drift of carriers toward the outer side of the nanowire.[7,10] We note that whereas the charge carrier drift is efficient during the first 100 ps of the decay, it is much slower for longer time delays. In particular, although we find a PL energy redshift rate of 160 μeV/ps in the first 100 ps, the redshift is only 37 μeV/ps between 400 and 800 ps time delays. Also, the PL energy 800 ps after the excitation pulse is 1.409 eV, a value that is still 52 meV larger than that measured in Figure 2d for continuous excitation. This slow drift of carriers in bent nanowires may be related to the slow thermalization rate reported previously for charge carriers in GaAs and InP nanowires and is tentatively attributed to phonon scattering effects at the surface of the nanowires.[33,34] By comparison, the time evolution of the PL of straight GaAs/(Al,Ga)As nanowires has been previously reported.[34,35] In this case, for a sufficiently low excitation power where band filling effects do not occur, the GaAs core PL at zero time delay is centered at about 1.52 eV and redshifts with increasing time delay. The redshift of the core PL peak energy is typically about 10 meV and arises from charge carrier localization at stacking defects.[32] The time-resolved PL of our straight GaAs/AlAs/GaAs nanowires exhibits a similar behavior, redshifting by 7 meV between 0 and 800 ps delay. Time-resolved PL experiments on straight $GaAs/Al_{0.3}Ga_{0.7}As/Al_{0.5}In_{0.5}As$ nanowires reveal that the PL redshift between 0 and 800 ps time delay is about 18 meV, which is attributed to carrier localization at stacking defects (see SI). The much larger redshift of 50 meV observed in Figures 2e and S6 for the bent nanowires is thus due to the additional drift of charge carriers toward the region of the GaAs core under tensile strain.

The dependence of the GaAs core PL intensity at 10 K on the polarization of the excitation laser in backscattering geometry is shown in Figure 2f for straight and bent $GaAs/Al_{0.3}Ga_{0.7}As/Al_{0.5}In_{0.5}As$ core−multishell nanowires. While the emission from straight nanowires is independent of the laser polarization, bent nanowires show much stronger absorption for light polarized along the bending axis than for light polarized perpendicular to the bending axis. Nanowire optoelectronic devices have usually consisted of nanowires standing vertically on a substrate.[36−38] Bending thus offers the possibility to convert a nanowire device with an isotropic polarization response into a polarization sensitive photodetector. The anisotropy in light absorption exhibited by bent nanowires is a consequence of the antenna effect,[39] which results directly from the interface conditions for the electric field (see SI). Additionally, while the PL signal from the GaAs core of straight nanowires at 10 K is unpolarized, that of bent

DOI: 10.1021/acs.nanolett.7b05221
Nano Lett. 2018, 18, 2343−2350

nanowires is polarized along the bending axis, making these structures promising for polarized light emitting devices (Figure 2f). As discussed in the SI, not only the antenna effect, but also the variation in $\varepsilon_{\parallel}$ across the GaAs core may affect the PL polarization of bent nanowires.

We have shown that in nanowires bent by asymmetric shells, charge carriers drift toward the tensile-strained outer part of the nanowire core, and emission from the core is redshifted. These effects, a consequence of the spatially varying strain fields in bent nanowires, can be exploited for light emission with a novel heterostructure which includes an active region at the outer side of the nanowire core. Figure 3a shows a schematic of a nanowire cross section, in which InAs quantum dots (QDs) have been placed on the same side of the GaAs core as a 40 nm thick $Al_{0.5}In_{0.5}As$ bending layer. To promote the formation of InAs three-dimensional (3D) islands on the GaAs$\{1\bar{1}0\}$ nanowire sidewalls, we exploited the recently reported morphological instability induced by surfactant Bi.[40,41] The codeposition of In, Bi, and As_2 results in 3D island formation only on the facet on which the As_2 flux is most directly incident (see SI). This effect, which is a result of As adatom diffusion being negligible compared to In diffusion, allows QDs to be positioned on a single nanowire facet. While the strain state varies from facet to facet around a bent nanowire, placing the QDs solely on the outer (or inner) facet should not broaden the emission band of the QD ensemble.

Figure 3b displays an SEM image of as-grown GaAs/InAs/$GaAs/Al_{0.3}Ga_{0.7}As/Al_{0.5}In_{0.5}As$ core−multishell nanowires with the structure shown in Figure 3a. Because of the larger total diameter, these nanowires exhibit a larger bending radius than the nanowires from Figure 1 and 2 (6.5 ± 0.7 μm). The 10 K continuous-wave PL spectra taken from this sample is displayed in Figure 3c for an excitation power of 750 μW. For comparison, a PL spectrum from bent nanowires with the InAs QDs present on the compressively strained inner side of the GaAs core is also shown. For both samples with inner and outer QDs, the InAs deposition was carried out on straight GaAs nanowire cores following the same procedure, and the only difference between the samples is the location of the $Al_{0.5}In_{0.5}As$ bending layer relative to the QDs. We note that for straight nanowires with InAs QDs synthesized using the same Bi surfactant-induced growth approach, the dominant PL peak was shown to originate from recombination in an InAs wetting layer with the QD emission located 50−150 meV below the wetting layer peak.[41] Similarly, for the spectra in Figure 3c we attribute the main PL peak for each sample to the InAs wetting layer. We observe that the dominant peak from nanowires with outer QDs is redshifted compared to nanowires with inner QDs. More importantly, nanowires with outer QDs exhibit a prominent low energy shoulder at about 80 meV below the main peak, indicating the emission intensity in this range is more than an order of magnitude higher than that for the sample with inner QDs. To confirm that this shoulder arises from enhanced light emission from the InAs QDs, we investigate the PL at lower excitation power. Figure 3d presents PL spectra from the same samples as in Figure 3c in the energy range of 1.19−1.37 eV and for an excitation power of 8.7 μW. In both spectra, we observe sharp transitions, however, the transitions are much more intense and extend to lower energies for the sample with InAs QDs on the outer side of the GaAs core. This increased emission is consistent with an enhanced transfer of carriers to the QDs from the GaAs core, and the redshift is consistent with the QDs being located in a region of relative tensile strain. A high-resolution PL spectrum taken from the sample with outer QDs is depicted in the inset, exhibiting emission features with full width at half-maximum (fwhm) down to 260 μeV. We attribute these narrow

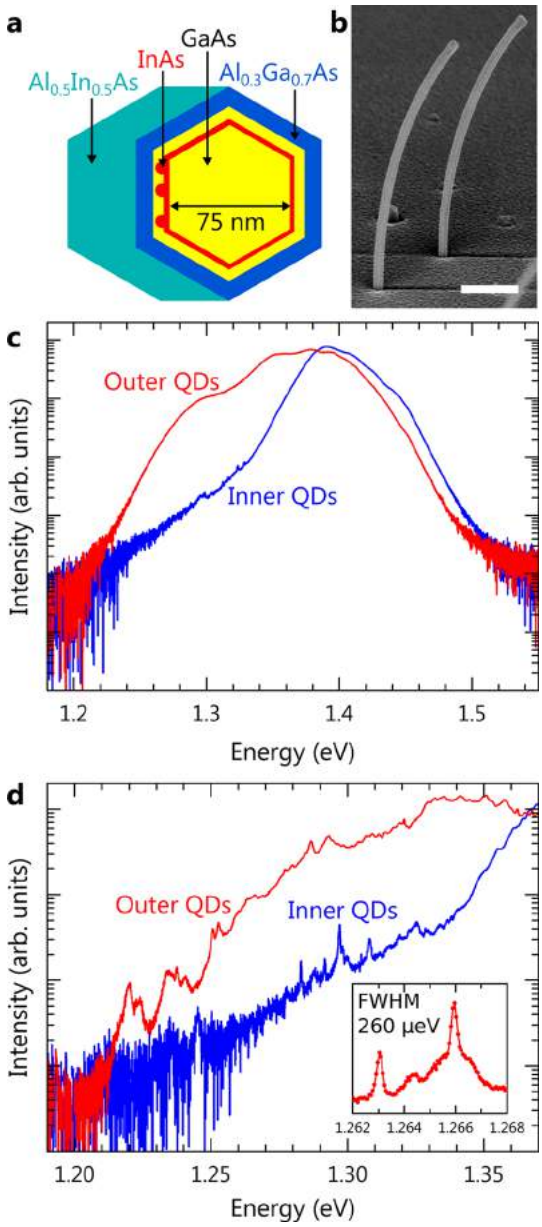

Figure 3. Bent-nanowire structures exploiting spatially varying strain fields for light emission. (a) Schematic cross-section of a bent-nanowire heterostructure incorporating InAs QDs on the tensilely strained outer side of a GaAs nanowire core (not to scale). (b) SEM image of as-grown nanowires with the structure as in (a). The scale bar corresponds to 1 μm. (c) PL spectra at 10 K from the nanowires in (b) (red line), as well as from bent nanowires with InAs QDs located on the compressively strained inner side of the GaAs core (blue line). The spectrum from nanowires with InAs on the outer side of the core is redshifted and shows a pronounced low-energy shoulder, compared to the other spectrum. The excitation power was 750 μW. (d) PL spectra from the same nanowires as in (c) acquired with a lower excitation power of 8.7 μW. The lower energy emission, attributed to emission from InAs QDs, is redshifted and more intense for the sample with outer InAs QDs. The inset displays a higher resolution spectrum from nanowires with outer InAs QDs at 1.4 μW excitation, exhibiting transitions with fwhm down to 260 μeV.

DOI: 10.1021/acs.nanolett.7b05221
Nano Lett. 2018, 18, 2343−2350

transitions to the recombination of excitons in individual InAs QDs, which merge to form the low energy shoulder observed at high excitation in Figure 3c. These findings demonstrate that even for moderate bending (see Figure 3b), the spatially varying strain fields in bent nanowires can dramatically increase the carrier capture of QDs placed in a region of tensile strain, resulting in more intense and redshifted emission. This is one example of how bent nanowires open up new possibilities for novel heterostructures with engineered spatially varying strain fields.

In summary, asymmetric lattice-mismatched shells can induce high degrees of controlled bending in nanowires. This new design freedom opens up many possibilities for exploitation in devices, including fabricating nanowire networks and interconnects, polarization sensitive light emitters and detectors, as well as light-emitting devices that exploit the spatially varying strain fields in bent nanowires. For example, quantum dot single-photon emitters embedded in nanowires can exploit bending to increase carrier collection by the quantum dots and to control the polarization and energy of emitted photons. These results highlight the vast potential for engineering unconventional spatially varying strain fields in flexible nanoscale heterostructures.

METHODS

Sample Growth. Samples were grown by MBE on n-type Si(111) wafers covered by an oxide mask 15−20 nm thick containing lithographically defined holes of about 40 nm diameter. The holes in the mask defined nanowire nucleation sites and were arranged in a hexagonal pattern with nearest neighbor separations ranging from 0.1 to 10 μm. The MBE was equipped with effusion cells for Ga, In, Al, and Bi and a valved cracker for supplying As_2, and the cells were inclined from the substrate normal by 33.5°. GaAs nanowire cores of about 4−5 μm length, 75 nm diameter and composed of 6 $\{1\bar{1}0\}$ sidewall facets were established using a two-step Ga-assisted vapor−liquid solid growth approach. The vertical yield of the GaAs nanowire cores was 30−40%. Details about the lithography and two-step core growth procedure can be found elsewhere.[42] Following core growth, the Ga droplets atop the nanowires were converted to GaAs by exposing the samples to an As_2 flux corresponding to four monolayers/s (ML/s) on planar GaAs(001) for 5 min. To realize the 45 nm diameter GaAs cores (from Figure 1), the 75 nm diameter GaAs cores were subsequently decomposed at 680 °C for 3 min (4.5 min for the cores in Figure 1h) in the absence of any flux (see SI).[43] $Al_{0.5}In_{0.5}As$ bending layers were deposited on the nanowires from one side at a substrate temperature of about 280 °C (455 °C in the case of the $GaAs/Al_{0.3}Ga_{0.7}As/Al_{0.5}In_{0.5}As$ series from Figure 2) with Al, In, and As_2 fluxes corresponding to 0.1, 0.1, and 4 ML/s on planar GaAs(001), respectively. Because of the different positions of the Al and In sources in the MBE chamber, Al and In could not be deposited simultaneously on the same side of the nanowires. To overcome this, the $Al_{0.5}In_{0.5}As$ layers were grown as a "digital alloy", whereby the substrate rotation angle was alternated between projecting either a $\langle 1\bar{1}0\rangle$ (nanowires in Figures 1 and 3) or a $\langle 11\bar{2}\rangle$ (nanowires in Figure 2) substrate direction toward the In and Al cells. The open time of each shutter was 2.5 s (corresponding to 0.05 nm of sidewall growth), and the total time of one sequence was 13 s. An As_2 flux of 4 ML/s was incident during the entire sequence. The projection of the group III flux on the nanowire sidewall varies with the inclination of the sidewall facet, which varies along the length of the nanowire and as the nanowire bends. Consequently, the deposited shell thickness will vary somewhat along the nanowire. However, we point out that the stress is determined by the bending radius, which is very homogeneous along the nanowire.

For the samples containing InAs QDs, the InAs deposition was carried out after core growth and droplet consumption and at a substrate temperature of 420 °C. To promote the formation of InAs QDs, a Bi flux of 0.4 ML/s was initiated 20 s before the InAs deposition and maintained throughout. The Bi flux acts as a surfactant[40] and was previously shown to induce the formation of InAs QDs on the $\{1\bar{1}0\}$ sidewalls of GaAs nanowires.[41] In was deposited for 17 s without substrate rotation at 0.1 ML/s. An As_2 flux of 4 ML/s was maintained throughout the Bi and In/Bi deposition steps. The configuration of the MBE sources resulted in the In and As_2 fluxes being incident on opposing sides of the nanowires. Under these conditions, we find that InAs 3D growth occurs on the side of the nanowires facing the As_2 source (see SI). Subsequent to InAs deposition, GaAs and $Al_{0.3}Ga_{0.7}As$ shells with respective thicknesses of 5 and 10 nm were deposited with Ga, Al, and As_2 fluxes corresponding to 0.23, 0.1, and 4 ML/s, respectively. The substrate was ramped to about 455 °C during the GaAs shell growth and rotated continuously at 0.17 Hz. Finally, the substrate temperature was reduced to about 280 °C and $Al_{0.5}In_{0.5}As$ bending layers of about 40 nm thickness were deposited as discussed above (282 sequences). The sample series without InAs QDs from Figure 2 was grown following a similar procedure, except that the Bi, InAs, and inner GaAs shell deposition steps were omitted, and $Al_{0.5}In_{0.5}As$ was deposited at about 455 °C instead of 280 °C. For the sample with conformal $Al_{0.5}In_{0.5}As$ shells, the substrate was rotated continuously during the deposition and Al, In, and As_2 were codeposited.

Photoluminescence Spectroscopy. Continuous-wave PL experiments were carried out at 10 K with a HeNe laser emitting at 632.8 nm, which was focused on the surface of the sample using a 0.25 N.A. microscope objective. The PL signal was collected using the same objective, sent to a 70 cm focal length spectrometer equipped with a 600 grooves per mm grating, and detected with a charge-coupled device camera cooled with liquid N_2. The orientation of the polarization of the excitation laser was rotated using a half-wave Fresnel rhomb retarder. The polarization of the PL signal was analyzed using a half-wave plate combined with a polarizer. Time-resolved PL spectroscopy was performed with pulses from an optical parametric oscillator pumped by a Ti:sapphire laser. The pulse wavelength, temporal width and repetition rate were 750 nm, 150 fs and 76 MHz, respectively. The energy fluence per pulse at the surface of the sample was about 200 $\mu J/cm^2$. The PL signal was dispersed spectrally using a 30 cm focal length spectrometer equipped with a 300 grooves per mm grating and temporally with a near-infrared sensitive streak camera operating in synchroscan mode, providing a temporal resolution of 20 ps. For time-resolved PL experiments on bent nanowires, the laser was polarized along the bending axis, whereas only emitted light cross-polarized to the laser was sent to the detector. For all PL experiments, the samples were mounted on the coldfinger of a continuous-flow He cryostat that can reach temperatures between 5 and 300 K.

DOI: 10.1021/acs.nanolett.7b05221
Nano Lett. 2018, 18, 2343−2350

■ ASSOCIATED CONTENT

Supporting Information

The Supporting Information is available free of charge on the ACS Publications website at DOI: 10.1021/acs.nanolett.7b05221.

Thermal decomposition of GaAs nanowires, top-view SEM images of bent nanowires, Bi-induced formation of InAs 3D islands on the {1$\bar{1}$0} sidewall facets of GaAs nanowires, analytical nanowire strain/bending calculations, time-resolved photoluminescence (PL) measurements, and optical anisotropies of bent group−III-As-based core−multishell nanowires (PDF)

■ AUTHOR INFORMATION

Corresponding Author

*E-mail: lewis@pdi-berlin.de.

ORCID

Ryan B. Lewis: 0000-0002-7216-3541

Pierre Corfdir: 0000-0003-0084-1187

Hanno Küpers: 0000-0001-8878-4644

Present Address

†(P.C.) ABB Corporate Research, 5405 Baden-Dättwil, Switzerland.

Author Contributions

R.B.L. and P.C. contributed equally. R.B.L and P.C. designed the experiments with contributions from L.G. and O.B. R.B.L. grew the samples with help from H.K. and carried out the SEM and strain investigations. P.C. carried out the PL study with help from T.F. for the time-resolved experiments. R.B.L. and P.C. composed the manuscript. All the authors discussed the results and commented on the manuscript.

Notes

The authors declare no competing financial interest.

■ ACKNOWLEDGMENTS

The authors are grateful to M. Höricke and C. Stemmler for MBE maintenance, O. Krüger and M. Matalla (Ferdinand-Braun-Institute Berlin) for e-beam lithography, B. Drescher, S. Rauwerdink, and A. Tahraoui for substrate preparation, and A. Hernández-Mínguez for a critical reading of the manuscript. R.B.L. acknowledges funding from the Alexander von Humboldt Foundation. P.C. acknowledges funding from the Fonds National Suisse de la Recherche Scientifique through Project No. 161032. This work was partially funded by Deutsche Forschungsgemeinschaft under grant Ge2224/2.

■ REFERENCES

(1) Ieong, M.; Doris, B.; Kedziersk, J.; Rim, K.; Yang, M. *Science* **2004**, *306* (5704), 2057−2060.

(2) Adams, A. R. *IEEE J. Sel. Top. Quantum Electron.* **2011**, *17* (5), 1364−1373.

(3) Jacobsen, R. S.; Andersen, K. N.; Borel, P. I.; Fage-Pedersen, J.; Frandsen, L. H.; Hansen, O.; Kristensen, M.; Lavrinenko, A. V.; Moulin, G.; Ou, H.; Peucheret, C.; Zsigri, B.; Bjarklev, A. *Nature* **2006**, *441* (7090), 199−202.

(4) Rudolph, J.; Hey, R.; Santos, P. V. *Phys. Rev. Lett.* **2007**, *99* (4), 047602.

(5) Nguyen, T. D.; Mao, S.; Yeh, Y. W.; Purohit, P. K.; McAlpine, M. C. *Adv. Mater.* **2013**, *25* (7), 946−974.

(6) Nam, D.; Sukhdeo, D. S.; Kang, J. H.; Petykiewicz, J.; Lee, J. H.; Jung, W. S.; Vučković, J.; Brongersma, M. L.; Saraswat, K. C. *Nano Lett.* **2013**, *13* (7), 3118−3123.

(7) Fu, X.; Su, C.; Fu, Q.; Zhu, X.; Zhu, R.; Liu, C.; Liao, Z.; Xu, J.; Guo, W.; Feng, J.; Li, J.; Yu, D. *Adv. Mater.* **2014**, *26* (16), 2572−2579.

(8) Dietrich, C. P.; Lange, M.; Klüpfel, F. J.; von Wenckstern, H.; Schmidt-Grund, R.; Grundmann, M. *Appl. Phys. Lett.* **2011**, *98* (3), 031105.

(9) Xu, S.; Guo, W.; Du, S.; Loy, M. M. T.; Wang, N. *Nano Lett.* **2012**, *12* (11), 5802−5807.

(10) Fu, X.; Jacopin, G.; Shahmohammadi, M.; Liu, R.; Benameur, M.; Ganière, J.-D.; Feng, J.; Guo, W.; Liao, Z.-M.; Deveaud, B.; Yu, D. *ACS Nano* **2014**, *8* (4), 3412−3420.

(11) Zhao, Y.; Yao, J.; Xu, L.; Mankin, M. N.; Zhu, Y.; Wu, H.; Mai, L.; Zhang, Q.; Lieber, C. M. *Nano Lett.* **2016**, *16* (4), 2644−2650.

(12) Hilse, M.; Takagaki, Y.; Herfort, J.; Ramsteiner, M.; Herrmann, C.; Breuer, S.; Geelhaar, L.; Riechert, H. *Appl. Phys. Lett.* **2009**, *95* (13), 133126.

(13) Keplinger, M.; Kriegner, D.; Stangl, J.; Mårtensson, T.; Mandl, B.; Wintersberger, E.; Bauer, G. *Nucl. Instrum. Methods Phys. Res., Sect. B* **2010**, *268* (3−4), 316−319.

(14) Krogstrup, P.; Ziino, N. L. B.; Chang, W.; Albrecht, S. M.; Madsen, M. H.; Johnson, E.; Nygård, J.; Marcus, C. M.; Jespersen, T. S. *Nat. Mater.* **2015**, *14* (4), 400−406.

(15) Day, R. W.; Mankin, M. N.; Lieber, C. M. *Nano Lett.* **2016**, *16* (4), 2830−2836.

(16) Hetzl, M.; Winnerl, J.; Francaviglia, L.; Kraut, M.; Döblinger, M.; Matich, S.; Fontcuberta i Morral, A.; Stutzmann, M. *Nanoscale* **2017**, *9* (21), 7179−7188.

(17) Wallentin, J.; Jacobsson, D.; Osterhoff, M.; Borgström, M. T.; Salditt, T. *Nano Lett.* **2017**, *17* (7), 4143−4150.

(18) Lauhon, L. J.; Gudiksen, M. S.; Wang, D.; Lieber, C. M. *Nature* **2002**, *420* (6911), 57−61.

(19) Liang, Y.; Nix, W. D.; Griffin, P. B.; Plummer, J. D. *J. Appl. Phys.* **2005**, *97* (4), 043519.

(20) Trammell, T. E.; Zhang, X.; Li, Y.; Chen, L.-Q.; Dickey, E. C. *J. Cryst. Growth* **2008**, *310* (12), 3084−3092.

(21) Kavanagh, K. L. *Semicond. Sci. Technol.* **2010**, *25* (2), 024006.

(22) Salehzadeh, O.; Kavanagh, K. L.; Watkins, S. P. *J. Appl. Phys.* **2013**, *114* (5), 054301.

(23) Lewis, R. B.; Nicolai, L.; Küpers, H.; Ramsteiner, M.; Trampert, A.; Geelhaar, L. *Nano Lett.* **2017**, *17* (1), 136−142.

(24) Roura, P.; López-de Miguel, M.; Cornet, A.; Morante, J. R. *J. Appl. Phys.* **1997**, *81* (10), 6916−6920.

(25) Dick, K. A.; Deppert, K.; Larsson, M. W.; Mårtensson, T.; Seifert, W.; Wallenberg, L. R.; Samuelson, L. *Nat. Mater.* **2004**, *3* (6), 380−384.

(26) Dick, K. A.; Deppert, K.; Karlsson, L. S.; Larsson, M. W.; Seifert, W.; Wallenberg, L. R.; Samuelson, L. *MRS Bull.* **2007**, *32* (2), 127.

(27) Dalacu, D.; Kam, A.; Austing, D. G.; Poole, P. J. *Nano Lett.* **2013**, *13* (6), 2676−2681.

(28) Kang, J.-H.; Cohen, Y.; Ronen, Y.; Heiblum, M.; Buczko, R.; Kacman, P.; Popovitz-Biro, R.; Shtrikman, H. *Nano Lett.* **2013**, *13* (11), 5190−5196.

(29) Car, D.; Wang, J.; Verheijen, M. A.; Bakkers, E. P. A. M.; Plissard, S. R. *Adv. Mater.* **2014**, *26* (28), 4875−4879.

(30) Rieger, T.; Rosenbach, D.; Vakulov, D.; Heedt, S.; Schäpers, T.; Grützmacher, D.; Lepsa, M. I. *Nano Lett.* **2016**, *16* (3), 1933−1941.

(31) Bogardus, E. H.; Bebb, H. B. *Phys. Rev.* **1968**, *176* (3), 993−1002.

(32) Graham, A. M.; Corfdir, P.; Heiss, M.; Conesa-Boj, S.; Uccelli, E.; Fontcuberta i Morral, A.; Phillips, R. T. *Phys. Rev. B: Condens. Matter Mater. Phys.* **2013**, *87* (12), 125304.

(33) Tedeschi, D.; De Luca, M.; Fonseka, H. A.; Gao, Q.; Mura, F.; Tan, H. H.; Rubini, S.; Martelli, F.; Jagadish, C.; Capizzi, M.; Polimeni, A. *Nano Lett.* **2016**, *16* (5), 3085−3093.

(34) Corfdir, P.; Küpers, H.; Lewis, R. B.; Flissikowski, T.; Grahn, H. T.; Geelhaar, L.; Brandt, O. *Phys. Rev. B: Condens. Matter Mater. Phys.* **2016**, *94* (15), 155413.

(35) Rudolph, D.; Schweickert, L.; Morkötter, S.; Hanschke, L.; Hertenberger, S.; Bichler, M.; Koblmüller, G.; Abstreiter, G.; Finley, J. J. *New J. Phys.* **2013**, *15* (11), 113032.

DOI: 10.1021/acs.nanolett.7b05221
Nano Lett. 2018, 18, 2343−2350

(36) Kikuchi, A.; Kawai, M.; Tada, M.; Kishino, K. *Jpn. J. Appl. Phys.* **2004**, *43* (12A), L1524−L1526.
(37) Wallentin, J.; Anttu, N.; Asoli, D.; Huffman, M.; Aberg, I.; Magnusson, M. H.; Siefer, G.; Fuss-Kailuweit, P.; Dimroth, F.; Witzigmann, B.; Xu, H. Q.; Samuelson, L.; Deppert, K.; Borgstrom, M. T. *Science* **2013**, *339* (6123), 1057−1060.
(38) Krogstrup, P.; Jørgensen, H. I.; Heiss, M.; Demichel, O.; Holm, J. V.; Aagesen, M.; Nygard, J.; Fontcuberta i Morral, A. *Nat. Photonics* **2013**, *7* (4), 306−310.
(39) Wang, J.; Gudiksen, M. S.; Duan, X.; Cui, Y.; Lieber, C. M. *Science* **2001**, *293* (5534), 1455−1457.
(40) Lewis, R. B.; Corfdir, P.; Li, H.; Herranz, J.; Pfüller, C.; Brandt, O.; Geelhaar, L. *Phys. Rev. Lett.* **2017**, *119*, 086101.
(41) Lewis, R. B.; Corfdir, P.; Herranz, J.; Küpers, H.; Jahn, U.; Brandt, O.; Geelhaar, L. *Nano Lett.* **2017**, *17* (7), 4255−4260.
(42) Küpers, H.; Lewis, R. B.; Tahraoui, A.; Matalla, M.; Krüger, O.; Bastiman, F.; Riechert, H.; Geelhaar, L. 2017, ArXiv 1708.05596.
(43) Loitsch, B.; Rudolph, D.; Morkötter, S.; Döblinger, M.; Grimaldi, G.; Hanschke, L.; Matich, S.; Parzinger, E.; Wurstbauer, U.; Abstreiter, G.; Finley, J. J.; Koblmüller, G. *Adv. Mater.* **2015**, *27* (13), 2195−2202.

DOI: 10.1021/acs.nanolett.7b05221
Nano Lett. 2018, 18, 2343−2350